REMOVAL OF JEM SIGNAL BY ACCURATE ESTIMATION OF INITIAL PARAMETERS OF CHIRPLET BASIS FUNCTIONS

Joo Ho Jung[1], Kyung Tae Kim[1], and Sang Hong Park[2, *]

[1]Department of Electrical Engineering, Pohang University of Science and Technology, Pohang, Gyungbuk, Korea

[2]Department of Electronic Engineering, Pukyong National University, Busan, Korea

Abstract—The inverse synthetic aperture radar (ISAR) image can be very effective in target recognition because it provides 2-D image that uses frequency data measured at various observation angles. However, the jet engine modulation (JEM) that can occur in the received signal due to the rotation of the blade in the engine may result in image blurring in cross-range direction. In this paper, we propose an efficient method of removing JEM signals by using the existing chirplet basis function and an efficient method to estimate the initial values of the four parameters of the chirplet. Simulations using the measured data provided clear ISAR image of a real Boeing747 aircraft.

1. INTRODUCTION

The inverse synthetic aperture radar (ISAR) image [1–3], which is an inverse mode of the synthetic aperture radar (SAR) [4], is a technique to derive the two dimensional (2D) radar cross section [5, 6] distribution of a target. The ISAR image is derived by synthesizing the reflected signals of the target at several aspect angles, generally measured by a fixed radar. Because this image can be utilized regardless of the conditions of weather, day and night, it is widely used by many military units for reconnaissance and recognition purposes along with the SAR, the range profile and the micro-Doppler [7, 8].

For the purpose of applying the ISAR image to the Korean military system, we recently conducted an intensive research on imaging and classification methods based on the range-Doppler algorithm (RDA) [9, 10]. Then, based on the principles derived, measurement was successfully conducted on a real Boeing747 aircraft by using the Korea miniature synthetic aperture radar (KOMSAR) with the support of Korean Agency for Defense Development. The measured data was processed using the RDA composed of range compression, range alignment, phase adjustment and cross-range compression, and a high resolution ISAR image was obtained which clearly represented the 2D scattering mechanism of the aircraft. However, the rotation of the blades in the engine caused inter-pulse phase difference called jet engine modulation (JEM). As a result, serious noise-like blurring occurred in the cross-range direction. This cross-range blurring can degrade the classification performance of the ISAR image. Therefore, it must be removed for successful classification. A recently proposed method removes JEM by using the adaptive chirplet representation [11]. This method derived the mathematical expansion of the cross-range signal for each range bin by using chirplet basis functions, removing the JEM signals whose frequency center and chirp rate are larger than those of the rigid body.

Although JEM signals can be removed successfully using the difference of parameters, it requires enormous computation time to estimate the four parameters of time window, time center, frequency center and chirp rate if the evolution-based algorithms such as genetic algorithms (GA) and particle swarm optimization (PSO) algorithms were used [9]. Recently, a fast refinement method (FRM) based on the gradient descent rule has been introduced [12]. However, this method assumes that a set of good initial parameters was guaranteed. Convergence of the chirplet expansion by this method often fails depending on the initial values of the parameters. Thus, for fast convergence, a new method is required that accurately estimates the initial parameters.

In this paper, we propose a method of accurately estimating the initial parameters for fast expansion of the signal into a sum of chirplet basis functions. The proposed method is capable of removing JEM signals efficiently. The proposed method utilizes the fast zooming algorithm (ZA) [13] for adaptive Gaussian representation and dynamically adjusts parameters if the expansion does not converge.

The results of our simulations on Boeing747 demonstrate that JEM signals are successfully removed, and clear ISAR images are derived in a relatively short computation time.

2. PRINCIPLES

2.1. Range-Doppler Algorithm

In this paper, we utilized the range-Doppler algorithm (RDA) which is a widely used method of ISAR imaging (Fig. 1) [1]. RDA makes use of the difference of Doppler frequency in the cross-range direction caused by the rotational component of a target. RDA is composed of three steps; range compression, translational motion compensation (TMC) composed of range alignment and phase adjustment, and cross-range compression [7, 8]. Range compression is the procedure to derive range profiles (RPs) that represent one dimensional (1D) distributions of scatterers by compressing the received radar signal using a matched-filter. TMC compensations for the inter-pulse translational movement of the target and the cross-range compression position each scatterer in the cross-range direction using the difference of Doppler frequency.
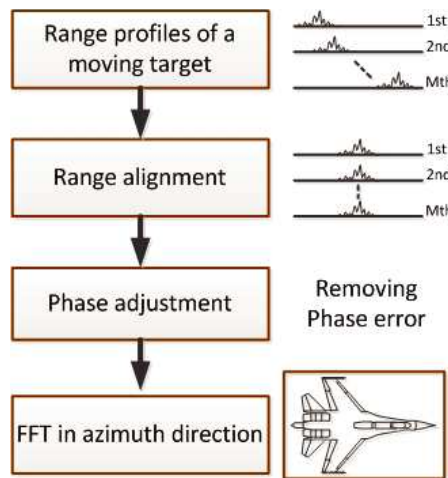
Figure 1. Procedure of RDA.

TMC is the most important procedure in ISAR imaging because the target is engaged in unnecessary translation motion in addition to the preferred rotational motion. Therefore, the observation points of each scatterer are different on the inter-pulse basis, and this obstructs the formation of focused ISAR images. TMC is composed of range alignment, and phase adjustment compensates for the translational motion and provides focused ISAR images. Range alignment is the procedure to align RPs to place each scatter at identical observation points using relative shift τ that minimizes 1D entropy function defined

by [2]

$$H_{G_m, G_{m+1}} = -\sum_{0}^{N-1} \bar{G}(\tau, n) \ln \bar{G}(\tau, n), \tag{1}$$

where

$$\bar{G}(\tau, n) = \frac{|G_m(n)| + |G_{m+1}(n - \tau)|}{\sum_{0}^{N-1} (|G_m(n)| + |G_{m+1}(n - \tau)|)}, \tag{2}$$

$G_m(n)$ and $G_{m+1}(n)$ are range profiles m and $m + 1$, and N is the total number of range bins. Phase adjustment removes residual phase errors caused by the range alignment, and 2D entropy function is used as a function defined as follows [2]:

$$Ent = \sum_{i=1}^{M} \sum_{j=1}^{N} |I(i, j)|^2 \ln |I(i, j)|^2 \tag{3}$$

where $I(i, j)$ is the $I(i, j)$th pixel value of the ISAR image and M is the number of RPs.

2.2. Signal Expansion Using the Chirplet Basis Function

The chirplet basis function is widely used in radar signal systems, seismic signal analysis and signal processing areas [13, 14]. The chirplet basis function is defined by

$$h_k(t) = \sqrt{\frac{\pi}{\alpha_k}} \exp\left(-\alpha_k(t - t_k)^2\right) \exp\left(-j2\pi f_k(t - t_k) - j\pi \beta_k(t - t_k)^2\right), \tag{4}$$

where α_k, t_k, f_k, and β_k are the inverse of the time window, time center, frequency center, and chirp rage, respectively. A signal can be represented by a sum of M chirplet basis functions with different parameters as follows [13, 14]:

$$s(t) = \sum_{k=1}^{M} A_k h_k(t), \tag{5}$$

where A_k is a constant derived by the inner product between $s_k(t)$ and $h_k(t)$. With $k = 0$ and $s_0(t) = s(t)$, which is the original signal, $s_k(t)$ is defined by

$$s_{k+1}(t) = s_k(t) - A_k h_k(t), \tag{6}$$

and $(\alpha_k, t_k, f_k, \beta_k)$ are the parameters that maximize the inner product defined as follows:

$$(\alpha_k, t_k, f_k, \beta_k) = \arg\max \left| \int_{-\infty}^{\infty} s_k(t) h_k(t) dt \right|, \tag{7}$$

(6) and (7) are repeated until the total energy of $s_{k+1}(t)$ is less than a predetermined limit. It was proven that (6) converges to 0 as k goes to infinity [13, 14].

2.3. Time-frequency Characteristics of a Rotating Scatterer

This paper utilizes the conclusion reached in [15] based on the signal modeling for ISAR imaging that includes the JEM signal. Assuming that a target is composed of the rigid body rotating with an angular velocity ω_B and the blade with ω_R ($\omega_R \gg \omega_B$) and that TMC has been successfully conducted, f_k and β_k of a scatterer m of the rigid body located at (x_m, y_m) and those of a scatter n of a blade at (x_n, y_n) can be represented by two groups of ellipsoids as follows [15]:

$$\frac{f_k^2}{(l_n\omega_R)^2} + \frac{\beta_k^2}{(l_n\omega_R)^2} = \left(\frac{2f_c}{c}\right)^2, \tag{8}$$

where $l_m = \sqrt{x_m^2 + y_m^2}$, $l_n = \sqrt{x_n^2 + y_n^2}$, f_c is the center frequency of the radar. Because ω_R is much larger than ω_B in (8), the rigid body is located near the origin and the blade is far from it in (f_k, β_k) domain. Therefore, for each range bin, JEM signals caused by the blade can successfully be removed if the cross-range radar signal is represented by (5), components near and far from the origin are properly clustered and the chirplet functions in each cluster are summed up again (Fig. 2).
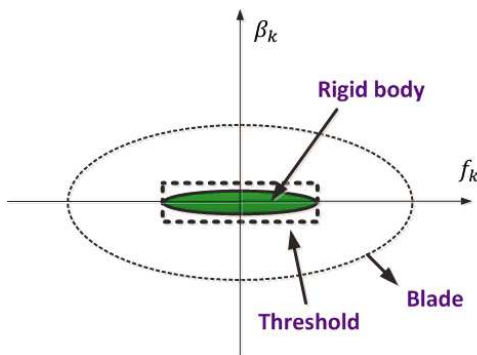
Figure 2. Separation of the body and the JEM signal [11].

2.4. Efficient Estimation of Chirplet Parameters

As mentioned above, JEM signals can be successfully removed by removing the chirplet functions having large (f_k, β_k) values when the

cross-range signal is expressed by a sum of chirplet functions. However, finding chirplet parameters in (4) is very difficult because (7) is a four dimensional (4D) optimization. Although the population-based algorithms such as GA and PSO may provide an optimized solution, enormous computation time can be consumed to find every $(\alpha_k, t_k, f_k, \beta_k)$.

In this paper, we apply the FRM for adaptive chirplet representation proposed in [12]. This method derives the parameters by curve-fitting in the 4D search space, and the convergence of (5) is very fast if a set of good initial parameters are supplied; the short time Fourier transform with a coarse time-frequency sampling grid is utilized in [12] for the estimation of the initial parameters. However, if the initial parameters are not proper, A_k provided by $(\alpha_k, t_k, f_k, \beta_k)$ can be a local minimum, and as a result, (6) can fail to converge. In addition, when the spectrum is distributed in a narrow time-frequency region, deriving the parameters for every grid can be ineffective and consume much computation time because (6) can converge using a small number of iterations conducted near the large spectrum values. Therefore, a good initial point is the prerequisite for the fast convergence of this method.

The method proposed in this paper to estimate the initial parameter is based on the ZA which is a stage-by-stage approach algorithm to estimate the Gaussian basis function given as follows [13]:

$$g_k(t) = \sqrt{\frac{\pi}{\alpha_k}} \exp\left(-\alpha_k(t - t_k)^2\right) \exp\left(-j2\pi f_k\left(t - t_k\right)\right), \qquad (9)$$

Note that $g_k(t)$ is $h_k(t)$ with $\beta_k = 0$. Starting from the center of the entire time span, this method sequentially divides the variance $\frac{1}{\alpha_k}$ of $g_k(t)$ and the time increment Δt_k. Then, among t_k and $t_k \pm \Delta t_k$, the time and f_k that maximize the absolute value of the Fourier transform of the product between $g_k(t)$ and $s_k(t)$ are sought. This procedure is
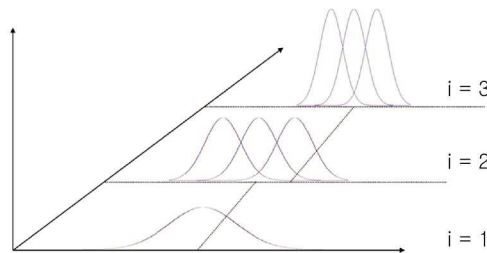
Figure 3. Principle of zooming algorithm.

repeated until the maximum absolute value no longer increases and α_k, t_k and f_k are selected (Fig. 3).

However, ZA does not always provide initial parameters that make (6) convergent. For example, in a test using a frequency-hopping signal having three frequencies, (6) was convergent by the Gauss functions given in Fig. 4(a), whereas those in Fig. 4(b) did not converge (6). Because Figs. 4(a) and (b) were formed by different α_k and t_k, it is required to dynamically adjust these two values if (6) does not converge. In this paper, if E_{k+1}, which is the energy of $s_{k+1}(t)$,

(a)   (b)
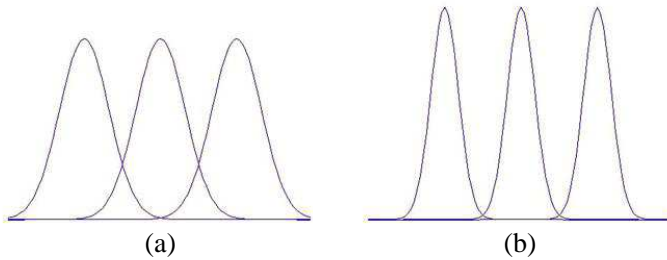
Figure 4. Convergent and non-convergent Gauss functions. (a) Convergent. (b) Non-convergent.
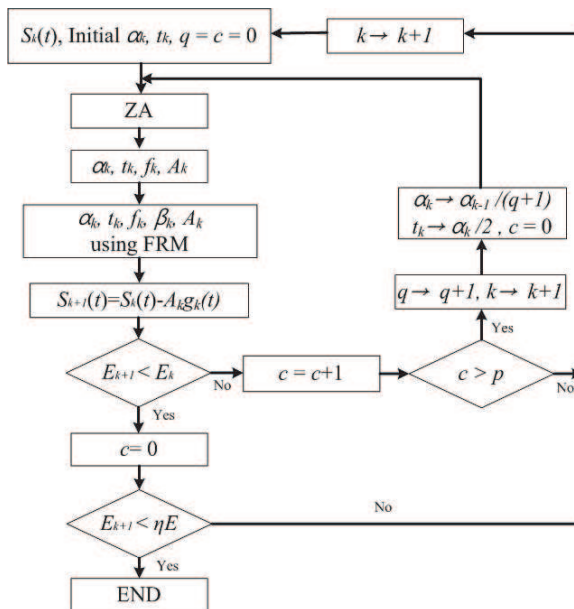
Figure 5. Proposed method for chirplet decomposition.

is larger than the energy E_k of $s_k(t)$ for p iterations, i.e., $s_{k+1}(t)$ does not converge for p iterations, and E_{k+1} is larger than η times the total energy E of $s(t)$, a new chirplet decomposition starts with α_k replaced by $\frac{\alpha_k}{(1+q)}$, where q is the number of failures in convergence. t_k is replaced by $\frac{\alpha_k}{2(1+q)}$. If $E_{k+1} < E_k$, p is set to 0 and the iteration continues, and this procedure is repeated until $E_{k+1} < \eta E$ (see Fig. 5).

3. SIMULATION RESULTS

The raw ISAR data of a real Boeing747 was measured in the Gimhae International Airport (http://www.airport.co.kr/doc/gimhae/) using the KOMSAR equipment whose parameters are summarized in Table 1. Two ISAR images were constructed using RDA for the demonstration of the proposed method, and each image was derived using 274 pulses; 300∼573th pulses and 2500∼2773th pulses for images 1 and 2 (Fig. 6).

Table 1. Radar parameters used for measurement.

Radar parameter	Value
Pulse repetition frequency	2 kHz
Pulse width	5 μs
Carrier frequency	X-band
Bandwidth	100 MHz
Resolution	1.5 m
Sampling frequency	150 MHz
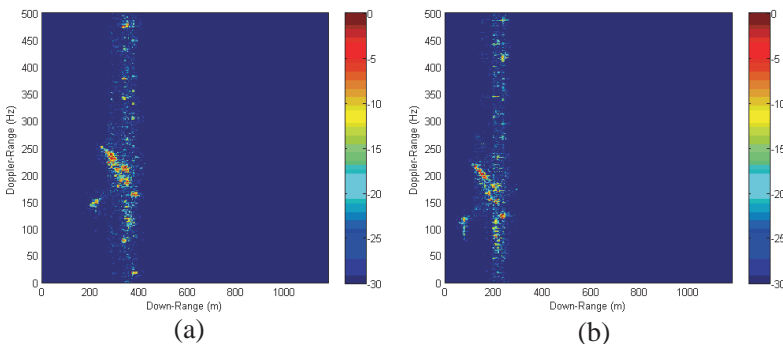
Figure 6. Two ISAR image of Boeing 747. (a) Image 1 (300∼573th pulses). (b) Image 2 (2500∼2773th pulses).

In estimating chirplet parameters, $p = 3$ and $\eta = 0.05$ were used, which means α_k and t_k are divided by 2 and the β_k is found again by using FRM if the energy of $s_k(t)$ did not increase as much as previous three iterations. In addition, iteration was stopped when E_{k+1} was smaller than 5% of E. The initial values applied to ZA using the cross-range signal for all range bins are $\alpha_k = 137$, which is a half of the number of pulses, $t_k = 137$ and $\Delta t_k = 137/2 = 67.5$. In the simulation that used the cross-range signal in the 60th range bin, failures on the convergence of (5) occurred 4 times due to the poor initial values found by ZA (see Fig. 7).

By using the threshold values $0 \leq \omega \leq 0.4\pi$ and $|\beta| \leq 0.002$, JEM signals of the two ISAR images in Fig. 6 were successfully removed
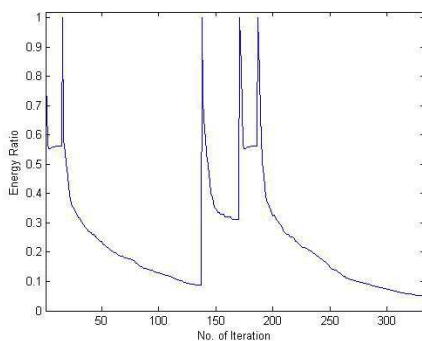
Figure 7. Convergence curve of Fig. 6(a).
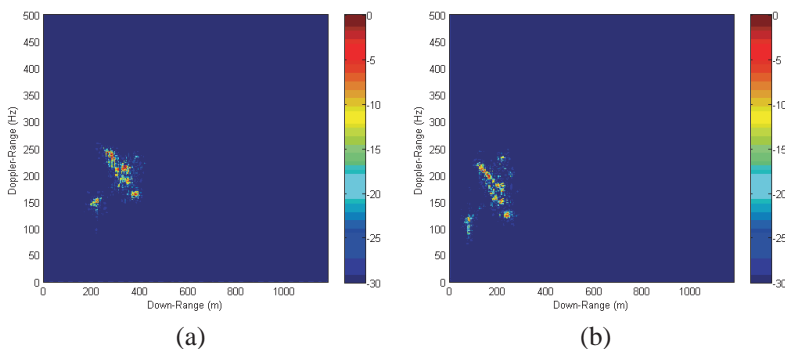
Figure 8. JEM-removed ISAR images. (a) Image 1 (300~573th pulses). (b) Image 2 (2500~2773th pulses).

by the proposed method (Fig. 8). The simulation was conducted using the Intel i7 processor, and the two ISAR images in Fig. 8 were derived within 10 s; those in Fig. 8(a) within 8.52 s and those in Fig. 8(b) within 6.39 s. The computation time may be further reduced if parallel processing technic is used with several processors which are generally installed in modern multifunctional radars. This demonstrates that the proposed method can be applied to the real-time target recognition. Some residual JEM signals remain near the nose of the aircraft as shown in Fig. 8(b) due to the threshold value, and they can be removed by readjusting the threshold values. However, because readjusting the threshold value can be another computational burden, the optimum threshold value should be predetermined. Therefore, determining the optimum threshold that can be used regardless of ISAR images is another topic for successful removal of JEM signals using chirplet basis functions. Comparison of the ISAR images in Fig. 6 and Fig. 8 in terms of the 2D entropy also demonstrates that the proposed method improves the quality of the ISAR images after JEM removal; 2D entropy of Fig. 6(a) improved from 7.1452 to 6.1659 and that of Fig. 6(b) from 7.116 to 6.39 (Table 2).

Table 2. Comparison of 2D entropy.

ISAR image (before JEM removal)	2D entropy	ISAR image (after JEM removal)	2D entropy
Fig. 6(a)	7.1452	Fig. 8(a)	6.1659
Fig. 6(b)	7.116	Fig. 8(b)	6.39

4. CONCLUSION

In this paper, we proposed an efficient method to remove JEM signals of Boeing747 aircraft measured by the KOMSAR equipment using the chirplet basis function. To resolve the difficult task of finding the initial four parameters for FRM which make the chirplet decomposition converge, the proposed method found four parameters using the ZA with an iterative adjustment of α_k and t_k; α_k and t_k were iterative changed when the signal energy did not decrease for p iterations. In simulations where the two ISAR images derived from the measured signal of Boeing747 are used, JEM signals were successfully removed and the 2D entropy that shows the image focus was considerably improved. In addition, the processing time of less than 10 s proved that the proposed method is capable of carrying out real-time automatic target recognition.

ACKNOWLEDGMENT

REFERENCES

1. Chen, C. C. and H. C. Andrews, "Target-motion-induced radar imaging," *IEEE Trans. Aerosp. Electron. Syst.*, Vol. 16, No. 1, 2–14, Jan. 1980.

2. Park, S.-H., M.-G. Joo, and K.-T. Kim, "Construction of ISAR training database for automatic target recognition," *Journal of Electromagnetic Waves and Applications*, Vol. 25, Nos. 11–12, 1493–1503, 2011.

3. Park, S.-H., K.-K. Park, J.-H. Jung, H.-T. Kim, and K.-T. Kim, "Construction of training database based on high frequency RCS prediction methods for ATR," *Journal of Electromagnetic Waves and Applications*, Vol. 22, Nos. 5–6, 693–703, 2008.

4. Chen, J., S. Quegan, and X. Yin, "Calibration of spaceborne linearly polarized low frequency SAR using polarimetric selective radar calibrators," *Progress In Electromagnetics Research*, Vol. 114, 89–111, 2011.

5. Zhu, X., W. Shao, J.-L. Li, and Y.-L. Dong, "Design and optimization of low RCS patch antennas based on a genetic algorithm," *Progress In Electromagnetics Research*, Vol. 122, 327–339, 2012.

6. Xu, H.-Y., H. Zhang, K. Lu, and X.-F. Zeng, "A holly-leaf-shaped monopole antenna with low RCS for UWB application," *Progress In Electromagnetics Research*, Vol. 117, 35–50, 2011.

7. Park, S.-H., "Automatic recognition of targets in formation using range profiles," *Journal of Electromagnetic Waves and Applications*, Vol. 26, Nos. 14–15, 2059–2069, 2012.

8. Park, J.-H., H. Lim, and N.-H. Myung, "Modified Hilbert-Huang transform and its application to measured micro Doppler signatures from realistic jet engine models," *Progress In Electromagnetics Research*, Vol. 126, 255–268, 2012.

9. Park, S.-H., H.-T. Kim, and K.-T. Kim, "Stepped-frequency ISAR motion compensation using particle swarm optimization with an island model," *Progress In Electromagnetics Research*, Vol. 85, 25–37, 2008.

10. Park, S.-H., K.-K. Park, J.-H. Jung, K.-T. Kim, and H.-T. Kim, "ISAR imaging of multiple targets using edge detection and Hough

transform," *Journal of Electromagnetic Waves and Applications*, Vol. 22, Nos. 2–3, 365–373, 2008.

11. Li., J. and H. Ling, "Application of adaptive chirplet representation for ISAR feature extraction from targets with rotating parts," *IET Proc. Radar Sonar Navi.*, Vol. 150, No. 4, 284–291, Aug. 2003.

12. Yin, Q., S. Qian, and A. Feng, "A fast refinement for adaptive gaussian chirplet decomposition," *IEEE Trans. Signal Processing*, Vol. 50, No. 6, 1298–1306, Jun. 2002.

13. Qian, S. and D. Chen, *Joint Time-frequency Analysis: Methods and Applications*, Prentice Hall, 1996.

14. Qian, S. and D. Chen, *Time-frequency and Wavelet Transforms*, Prentice Hall, 2002.

15. Bultan, A., "A four-parameter atomic decomposition of chirplets," *IEEE Trans. Signal Processing*, Vol. 47, No. 3, 731–745, Mar. 1999.